# UC Berkeley
## UC Berkeley Previously Published Works

**Title**

Versatile Core–Shell Nanoparticle@Metal–Organic Framework Nanohybrids: Exploiting Mussel-Inspired Polydopamine for Tailored Structural Integration

**Permalink**

https://escholarship.org/uc/item/7gt957wc

**Journal**

ACS Nano, 9(7)

**ISSN**

1936-0851

**Authors**

Zhou, Jiajing
Wang, Peng
Wang, Chenxu
et al.

**Publication Date**

2015-07-28

**DOI**

10.1021/acsnano.5b01138

Peer reviewed

# Versatile Core–Shell Nanoparticle@Metal–Organic Framework Nanohybrids: Exploiting Mussel-Inspired Polydopamine for Tailored Structural Integration

**Jiajing Zhou**[†], **Peng Wang**[†,‡], **Chenxu Wang**[†], **Yi Ting Goh**[†], **Zheng Fang**[†], **Phillip B. Messersmith**[§], and **Hongwei Duan**[†,*]

[†]School of Chemical and Biomedical Engineering, Nanyang Technological University, 70 Nanyang Drive, Singapore 637457

[‡]Nanyang Environment and Water Research Institute (NEWRI), Nanyang Technological University, 1 Cleantech Loop, Singapore 637141

[§]Bioengineering and Materials Science and Engineering Departments, University of California, Berkeley, California 94720-1760, United States

## Abstract

We report a versatile strategy based on the use of multifunctional mussel-inspired polydopamine for constructing well-defined single-nanoparticle@metal–organic framework (MOF) core–shell nanohybrids. The capability of polydopamine to form a robust conformal coating on colloidal substrates of any composition and to direct the heterogeneous nucleation and growth of MOFs makes it possible for customized structural integration of a broad range of inorganic/organic nanoparticles and functional MOFs. Furthermore, the unique redox activity of polydopamine adds additional possibilities to tailor the functionalities of the nanohybrids by sandwiching plasmonic/catalytic metal nanostructures between the core and shell *via* localized reduction. The core–shell nanohybrids, with the molecular sieving effect of the MOF shell complementing the intrinsic properties of nanoparticle cores, represent a unique class of nanomaterials of considerable current interest for catalysis, sensing, and nanomedicine.

## Graphical Abstract

[*]Address correspondence to: hduan@ntu.edu.sg.
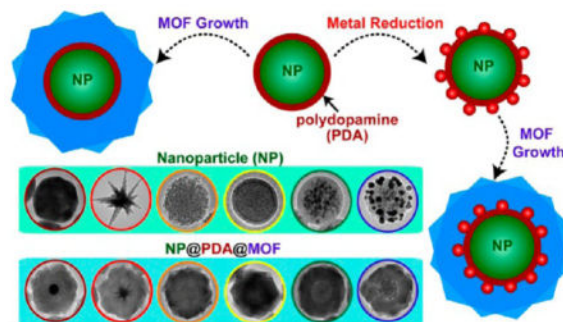
## Keywords

mussel-inspired polydopamine; metal–organic framework; core–shell nanostructure; nanohybrid; recyclable nanocatalyst

In this article, we report a generally applicable strategy that allows for constructing heterogeneous core–shell nanostructures with a customized selection of functional nanoparticle core and metal–organic frameworks (MOFs) shell. The ability to control structural integration of functional materials at nanometer scale opens the access to heterogeneous nanohybrids with collective properties that are not available in individual building blocks.[1–3] Emerging properties of the heterogeneous nanohybrids hold great promise in catalysis, theranostics, and combination therapy, in which the synergistic action of multiple components is necessitated for optimal performance.[4–9] The structure-dependent optical, electrical, magnetic, and catalytic properties of metal, semiconductor, and metal oxide nanoparticles have stimulated intense research and developments in chemistry, materials sciences, biology and medicine.[10] MOFs are an intriguing class of microporous crystalline materials built upon coordinated metal ions and organic ligands.[11] The readily tunable microporous structures and functionalities of MOFs, deriving from a diverse collection of available building blocks, underpin their applications in molecular storage and separation, chemical sensing, and catalysis.[12–18] There is growing interest in developing nanoparticle@MOF core–shell nanohybrids to complement nanoparticle functionality with the molecular sieving effect of MOFs, imparted by their defined pore apertures.[19,20] Although considerable progress has been made, the majority of existing methods, by means of either *in situ* synthesis of nanoparticles inside MOFs[21–24] or depositing MOF coatings on preformed nanoparticles,[25–29] mainly give rise to hybrid materials with many nanoparticles dispersed in the MOF matrix rather than well-defined core–shell nanostructures with a layer of MOF sealing off a single nanoparticle core. More recently, several groups have reported that selective nanoparticle capping ligands such as poly-vinylpyrrolidone (PVP) can mediate the deposition of a MOF shell on metal nanoparticles to form core–shell nanohybrids.[30–35]

Here we show that the use of an intermediate mussel-inspired polydopamine (PDA) coating opens new possibilities for tailored synthesis of core–shell nanoparticle@MOF nanohybrids. Self-polymerization of dopamine in the presence of virtually any solid substrate leads to a stable and conformal PDA coating that is bound to the substrate through covalent and/or noncovalent interactions.[36–42] A unique combination of physicochemical characteristics of

PDA plays critical roles in the success of our strategy, as illustrated in Scheme 1. First, the adhesive nature and controllable growth kinetics of PDA makes it possible to form a conformal layer of PDA with controlled thickness on a wide spectrum of nanoparticles of different chemical identities and functionalities. Second, metal-chelating activity of the catechol groups[43–45] in PDA can drive the heterogeneous nucleation and growth of MOFs on PDA coated nanoparticles, affording exclusively the core–shell nanohybrids. Importantly, the PDA coating endows the nanoparticle cores with excellent colloidal stability, which prevents nanoparticles from aggregating in MOF growth solution. Third, the redox reactivity of PDA[46–48] enables localized reduction of metal precursors, which leaves metal nanostructures sandwiched between the nanoparticle core and MOF shell, providing unique opportunities for constructing multi-functional nanohybrids. We have demonstrated that our strategy allows controlled growth of classical MOFs on a broad range of inorganic and organic nanostructures, offering unprecedented chemical flexibility in developing core–shell nanohybrids. A prototypical example illustrated here involves loading catalytic Au nanoparticles in MOF-coated magnetic nanoparticles by taking advantage of the redox activity of PDA. Complementary properties of the multiple components of the nanohybrids give rise to magnetically recyclable nanocatalysts with molecular size selectivity.

## RESULTS AND DISCUSSION

Au nanoparticles with localized surface plasmon resonance (LSPR) highly sensitive to the change of their surrounding dielectric environment and aggregation status are excellent model core materials that can provide real-time colorimetric feedback on the successful loading of shell coatings.[49,50] Here the deposition of PDA on Au nanoparticles of 50 nm was conducted in freshly prepared dopamine solution in Tris buffer (10 mM, pH 8.5). Afterward, the nanoparticles can be separated by centrifugation and redispersed in NaCl solution (0.15 M) and methanol, indicating a considerable change in surface properties (Figure S1). In contrast, the citrate-stabilized Au nanoparticle without PDA coating formed large aggregates and quickly precipitated, as indicated by the irreversible red to blue color change of the nanoparticle dispersion (Figure S1). In transmission electron microscopy (TEM) images (Figure 1a,d), a PDA coating of lower contrast surrounding the Au nanoparticles can be easily identified. We have found that the thickness of PDA shell is highly dependent on the dopamine concentration. While 0.25 mg/mL dopamine led to a uniform PDA coating of 6 nm after reacting with Au nanoparticles (0.2 nM) for 18 h, increasing the concentration to 0.5 mg/mL gave rise to a thickness of 25 nm, as observed in Figure 1a,d. We next examined the growth of a representative zeolitic imidazole framework material (ZIF-8) on PDA coated Au nanoparticles (AuNP@PDA). ZIF-8 building blocks, $Zn(NO_3)_2$ (12.5 mM) and 2-methylimidazole (25 mM), were mixed with the AuNP@PDA dispersion in methanol, and the product was collected after 12 h. TEM image (Figure 1b) of the pink-red products clearly shows a homogeneous layer (40 nm) of ZIF-8 crystal on top of the AuNP@PDA nanoparticles. And a thicker layer of ZIF-8 of 90 nm (Figure 1c) was produced when we doubled the concentration of the precursors. Notably, when the AuNP@PDA nanoparticles with 25 nm PDA shell were used, two concentric layers around the Au nanoparticle cores (Figure 1e) were evidently observed after the ZIF-8 growth, suggesting that ZIF-8 nucleated rapidly on the surface of PDA coating and subsequently grew into larger nanocrystals. The

strong chelating power of residual catechol groups in PDA and the hydrophobic interaction between aromatic groups of PDA and the organic ligands both are expected to facilitate rapid nucleation, leading to high yield of the well-defined core–shell nanohybrids. Scanning electron microscopy (SEM) observation (Figure 1f) further confirmed its homogeneous size distribution across a large population.

Figure 2a shows that the LSPR peak of 50 nm Au nanoparticles red-shifted from 535 to 560 nm in AuNP@PDA, and further moved to 580 nm after the ZIF-8 shell was deposited to form the core–shell nanohybrids, because of the higher refractive index of PDA and ZIF-8 than that of water. Time-dependent UV–vis spectroscopy measurements reveal that the LSPR redshifts primarily occurred in the first 3 min of ZIF-8 growth (Figure S2), which is in line with the rapid nucleation and growth of the MOF deduced from the TEM observation (Figure 1e). ZIF-8 represents an easily synthesized MOF material that is formed rapidly under ambient condition. We have found that UiO-66, which is solvothermally prepared using 1,4-benzenedicarboxylic acid ($H_2BDC$) as organic linkers and zirconium-(IV) as metal cores, can also be readily coated on AuNP@PDA (Figure 2b), indicative of the compatibility of the PDA-based strategy with other synthesis conditions and a diverse range of functional groups found in MOF building blocks. X-ray diffraction (XRD) patterns of both AuNP@PDA@MOF core–shell nanohybrids display the characteristic peaks of face-centered-cubic phase of Au and ZIF-8 or UiO-66 crystals, confirming the high loading of nanocrystals in the core–shell configuration. The type I $N_2$ isotherm revealed in nitrogen-sorption measurements is suggestive of the microporosity of the core–shell nanohybrids. In comparison with the pure nanosized ZIF-8 and UiO-66 (Figure S3), which show gravimetric Brunauer–Emmett–Teller (BET) surface areas of 1541 and 1496 $m^2\ g^{-1}$ respectively, the core–shell AuNP@ PDA@ZIF-8 and AuNP@PDA@UiO-66 nanohybrids exhibit smaller surface areas of 1082 and 1353 $m^2\ g^{-1}$, resulting from the introduction of nonporous Au core in the hybrids (Figure 2d).

To examine the compatibility of the PDA-based method with nanoparticle cores of different morphologies, anisotropic Au nanostars were used for preparing the core–shell nanohybrids. Au nanostars with sharp tips were prepared by a seeded-growth method on 14 nm Au nanoparticles (Figure 3a).[51] Regardless of the anisotropic structure and different surface property of Au nanostars compared to Au nanoparticles, a PDA layer can also be coated on Au nanostars (Figure 3b). TEM image shows that ZIF-8 crystal was readily grown on PDA coated Au nanostars of 80 nm (Figure 3c), forming core–shell structures with the nanostars completely trapped inside the ZIF-8 shell. Similar to that of the spherical Au nanoparticles, the broad LSPR peak of Au nanostars at 826 nm red-shifted to 897 and 913 nm after PDA and ZIF-8 layers were introduced.

This strategy is also valid for cores of different chemical composition. Mesoporous silica nanoparticles (MSNs)[52] and polystyrene nanoparticles (PSNs)[53] were selected as representative inorganic oxide and organic nanomaterials, which are also under intense research for a broad spectrum of applications.[8,54] Following the similar protocol developed for Au-based nanomaterials, we were able to successfully coat ZIF-8 of a controlled layer thickness on both MSNs and PSNs. TEM observation (Figure 4) confirmed that the successive coating of PDA and MOF layers can also be done on MSNs and PSNs, leading to

well-defined core–shell structures. Taken together, the generation of a robust PDA coating by self-polymerization of dopamine is not dependent on the nature of the underlining substrates, and the PDA-enabled strategy allows customized structural integration of functional nanostructures and MOFs.

The general applicability of this strategy opens the access to diverse core–shell nanoparticles with the functionality of the core nanoparticles complementing molecular size selectivity of the MOF shell. Polystyrene-trapped magnetic iron oxide nanoparticles (MagNPs) were prepared by emulsion polymerization.[54,55] A core of magnetic iron oxide nanoparticles is clearly visible within the polystyrene nanobead (Figure 5a). The growth of PDA and ZIF-8 shell gave rise to obvious size increase, forming core–shell nanoparticles with their MagNP core and ZIF-8 shell easily identified in TEM images (Figure 5b,c). Because of the addition of nonmagnetic PDA and MOF components, the resulting MagNP@PDA@ZIF-8 core–shell nanoparticle has a decreased magnetization saturation value of 3.1 emu/g in comparison with that of MagNP (33.2 emu/g) and MagNP@PDA (12.7 emu/g) (Figure 5d).[56]

Self-polymerization of dopamine proceeds *via* oxidation of catechol into dopaminequinone followed by intramolecular cyclization, further oxidative oligomerization and self-assembly, leaving behind abundant redoxactive catechol groups in PDA. Figure 6a shows that PDA coating on MagNPs is able to induce localized reduction of Au precursor, giving rise to a number of uniform Au nanoparticles of 15 nm in size loaded on PDA coating. It appears that the Au nanoparticles reside on the surface of PDA instead of trapped inside the PDA network. On the hand, no nanoparticles were formed when MagNPs without PDA coating underwent the same treatment (Figure S4). Furthermore, ZIF-8 and UiO-66 shells (Figure 6b,c) both can be coated on MagNPs carrying Au nanoparticles (MagNP@PDA@AuNPs), implying that the loading of Au nanoparticles did not affect the ability of PDA to mediate MOF growth (Figure S5). In UV–vis spectra (Figure 6d), the characteristic LSPR peak of AuNPs emerged after the localized reduction on PDA coated MagNPs, and remained in the MOF coated nanoparticles. The three-component MagNP@PDA@AuNPs@-MOF nanohybrids can be easily recovered by a magnetic field (inset of Figure 6d).

We next explored the application of the nanoparticle@ MOF core–shell nanohybrids with complement properties. Metal nanoparticles with large surface areas have emerged as a new class of catalysts that are receiving increasing attention. The MagNP@ PDA@AuNPs@MOF nanohybrids have built-in magnetic property from the MagNP core, catalytic activity from the loaded Au nanocatalysts, and molecular sieving effect from the MOF shell, which are collective characteristics necessitated for magnetically recyclable nanocatalysts with molecular size selectivity. The metal-catalyzed reduction of 4-nitrophenol (4-NPh) to 4-aminopheol (4-APh) and methylene blue (MB) to leuco MB (LMB) by $NaBH_4$ were selected as the model reactions to examine this potential of the core–shell nanohybrids. 4-NPh has strong absorption at 400 nm which disappears upon conversion into 4-APh, making it possible to follow the reaction using UV–vis spectroscopy.[36] In control experiments, ZIF-8 and UiO-66 themselves did not show any catalytic activity (Figure 7 and S6) for both reactions. As demonstrated in Figure 7a, while MagNP@PDA@AuNPs without MOF shell led to rapid conversion of 4-NPh into 4-APh, the reaction was completely inhibited when a layer of ZIF-8 was coated on the nanoparticles. Apparently, the small

aperture size of ZIF-8 (3.4 Å) prevented the diffusion of 4-NPh (~4.8 Å) through the MOF shell to access the Au nanocatalysts. In line with this analysis, the use of UiO-66 MOF shell with a larger aperture size (6.0 Å) did not affect the reaction significantly. The slight reduction of reaction rate possibly resulted from the limited diffusion of 4-NPh through the MOF shell.[28] Recycling nanoscale catalysts has been a significant challenge in the field. Our results demonstrate that the magnetically recycled nanohybrids maintained excellent colloidal stability and catalytic activity (Figure S7) in repeated uses. For the reduction of MB (Figure 7b), which has a molecular size of ~7.6 Å, it is apparent that even UiO-66 coated nanoparticles did not show any reaction activity due to diffusion inhibition caused by molecular selectivity of the MOF layer.

## CONCLUSION

In summary, we have presented a versatile, PDA-enabled strategy for developing well-defined nanohybrids consisting of a nanoparticle core and a MOF shell. The ability of PDA to adhere to colloidal substrates of any chemical composition and to bind with a wide spectrum of MOF building blocks forms the fundamental basis of our strategy, and its unique redox activity adds an additional dimension to customize the functionalities of the resultant core–shell nanohybrids. The general applicability of this new approach was highlighted with varieties of nanohybrids consisting of different nanoparticle and MOF pairs. In particular, nanohybrids with catalytic Au nanoparticles sandwiched between the magnetic core and MOF shell through localized reduction by PDA, as magnetically recyclable nanocatalysts with molecular size selectivity, have demonstrated the potential of our strategy for flexible, rational functionality integration. The full potential of this strategy in emerging fields such as nanomedicine and photocatalysis is to be realized by the introduction of new building blocks, fueled by recent advances in tailored synthesis of nanocrystals and functional MOFs. The core–shell nanohybrids with a molecular sieving effect added onto the intrinsic properties of the nanoparticle core are of considerable interest for controlled drug release and improved selectivity in sensing and catalysis applications.

## EXPERIMENTAL SECTION

### Materials

Dopamine, sodium citrate, hydroxylamine hydrochloride ($NH_2OH \cdot HCl$), hexadecyl trimethylammonium bromide (CTAB), sodium hydroxide (NaOH), tetraethyl orthosilicate (TEOS), $p$-styrenesulfonic acid sodium salt (NaSS), iron(III) chloride hexahydrate ($FeCl_3 \cdot 6H_2O$), iron(II) chloride ($FeCl_2 \cdot 4H_2O$), ammonium hydroxide, oleic acid, sodium dodecyl sulfate (SDS), styrene, tetradecane, potassium peroxydisulfate (KPS), zinc nitrate hexahydrate ($Zn(NO_3)_2$), 2-methy-limidazole, zirconium(IV) chloride ($ZrCl_4$), terephthalic acid ($H_2BDC$), acetic acid, 4-nitrophenol (4-NPh), methylene blue (MB) and sodium boronhydride ($NaBH_4$) were purchased from Sigma-Aldrich. Methanol (MeOH), ethanol (EtOH) and $N,N$-dimethylmethanamide (DMF) were obtained from Fisher Chemical. Hydrogen chloride (HCl) was obtained from Schedelco. Silver nitrate ($AgNO_3$) was acquired from Strem chemicals. L-Ascorbic acid (LAA) was obtained from Tokyo Chemical Industry. Hydrogen tetrachloroaurate(III) trihydrate ($HAuCl_4 \cdot 3H_2O$) was supplied by Alfa

Aesar. Tris(hydroxymethyl)aminomethane (TRIS) was obtained from J. T. Baker. Ultrapure water (18.2 MΩ · cm) was purified using a Sartorius AG arium system and used in all experiments.

### Characterization

Scanning electron microscopy (SEM) images were acquired on a FESEM (JSM-6700F, Japan). Transmission electron microscopy (TEM) observations were conducted on a Jeol JEM 2010 electron microscope at an acceleration voltage of 300 kV. UV–vis spectra were recorded using a Shimadzu UV1800 spectrophotometer. Powder X-ray diffraction (XRD) patterns were obtained on a Bruker AXS D2 Advanced X-ray diffractometer with monochromatized Cu Ka radiation ($\lambda$ = 1.54056 Å, 40 kV and 20 mA). BET surface area was measured by $N_2$ adsorption and desorption at 77 K using a Micromeritics ASAP 2020 apparatus.

### Synthesis of 50 nm Au Nanoparticles

50 nm AuNPs were prepared using a seeded-growth method. Typically, seed AuNPs with a diameter of 14 nm were prepared first. Five milliliters of 12 mg/mL sodium citrate solution were injected into a 50 mL boiling water solution containing 5 mg of $HAuCl_4$ under vigorous stirring. A color change from colorless to red was observed in 5 min. The solution was heated for another 20 min, and then cooled to room temperature before further use. This seed AuNP dispersion was used to synthesize 50 nm AuNPs. Briefly, 50 mL water was added into a 100 mL round-bottom flask. Two milliliters of seed AuNPs and 200 $\mu$L of 0.2 M $NH_2OH \cdot HCl$ were added into this flask consecutively. Afterward, 3 mL of 0.1 wt % $HAuCl_4$ was added dropwise into the solution under vigorous stirring followed by 30 min reaction at room temperature. A gradual color change from light red to dark red was observed. Finally, the concentration of sodium citrate was adjusted to 1 mM. The reaction was stopped after another 2 h and nanoparticle dispersion was stored at 4 °C for further use.

### Synthesis of Au Nanostars

To synthesize Au nanostars, 0.2 mL of 25 mM $HAuCl_4$ was added into 15 mL of $H_2O$, followed by 20 $\mu$L of 1 M HCl and 0.145 mL of 14 nm AuNP seeds. The solution was stirred for 2 min, and then 40 $\mu$L of 10 mM $AgNO_3$ was injected into the reaction. After 2–3 min, 100 $\mu$L of LAA (100 mM) was added rapidly. The solution turned green immediately once LAA was introduced. After another 2 min, 1 mL of CTAB (10 mM) was added into the mixture to stabilize the Au nanostars.

### Synthesis of MSNs

MSN was prepared by co-condensation method. CTAB (500 mg) was dissolved in DI water (240 mL) followed by the addition of NaOH aqueous solution (1.50 mL, 2 M). The mixture was heated up to 80 °C under $N_2$ in 500 mL round bottomed flask with vigorous stirring. When the temperature became stable, TEOS (2.5 mL) was slowly added into the mixture solution *via* syringe. The mixture became turbid after adding TEOS, and was then stirred at 80 °C for another 2 h. Afterward, nanoparticles were collected by centrifugation at 8000 rpm for 10 min. The product was washed with MeOH, DI water and MeOH thoroughly. CTAB

was removed by suspending the nanoparticles in MeOH (150 mL) containing HCl (3 mL, 37%). The mixture was refluxed at 80 °C for 24 h. The product MSNs were collected by centrifugation at 8000 rpm for 10 min and thoroughly washed by MeOH, water and MeOH.

### Synthesis of PSNs

The polystyrene nanoparticles were prepared by soap-free polymerization in the presence of NaSS. Distilled 10 g styrene, 0.0831 g of KPS, 90 mL of water, and NaSS were charged into the reactor and then deoxygenated with $N_2$ for 1 h. The reactant mixture was reacted at 70 °C for 24 h under $N_2$ atmosphere. The obtained PSNs were dialyzed against water before further use.

### Synthesis of MagNPs

$FeCl_3 \cdot 6H_2O$ (2.4 g) and $FeCl_2 \cdot 4H_2O$ (0.982 g) were dissolved in 10 mL DI water under $N_2$ gas with vigorous stirring at 80 °C. Then, 5 mL of ammonium hydroxide was added rapidly into the solution. The color of solution turned to black immediately. After 30 min, 3 mL of oleic acid was added and the suspension was kept at 80 °C for 1.5 h. The obtained magnetite nanoparticles were washed with water and MeOH until pH became neutral. Magnetite nanoparticles (0.5 g) were added into 12 mL of water containing 10 mg of SDS, and the mixture in ice–water bath was treated with ultrasound for 10 min to obtain miniemulsion of magnetite nanoparticles. A styrene emulsion was prepared using 5 mL of styrene, 50 mg of SDS, 40 mL of water, and 0.033 mL of tetradecane. Miniemulsion of magnetite nanoparticle and 5 mg of KPS were added to a three-neck flask and stirred for 30 min at 500–600 rpm in $N_2$ atmosphere. Afterward, 10 mL of styrene emulsion was added into the mixture, and the flask was placed in 80 °C water bath and maintained for 20 h to obtain MagNPs. This as-fabricated MagNPs was collected with a magnet and redispersed in $H_2O$, and the collection-redispersion cycle was repeated three times before dispersing the MagNPs in 10 mL of $H_2O$ for further usage.

### Nanoparticle@PDA Core–Shell Nanoparticles

Typically, 50 mL of as-synthesized 50 nm Au nanoparticles were centrifuged at 900 rcf for 15 min. Then, the pellets were redispersed in 2 mL of $H_2O$. 600 $\mu L$ of the concentrated AuNPs was dispersed in 16 mL of TRIS buffer (pH 8.5), followed by adding 10 mg of dopamine. The reaction solution was stirred for 18 h, and the purple product was purified by centrifugation. Similar procedure was applied to deposit PDA on other nanoparticles.

### Synthesis of MagNP@PDA@AuNPs

MagNP@PDA solution was injected into 50 mL of $H_2O$ at 85 °C under vigorous stirring. After 2 min, 4 mL of 0.1 wt % of $HAuCl_4$ was injected into the solution. The reaction solution was stirred for 15 min at 85 °C. The color of dispersion turned into dark brown first, and then became red finally. After purified by centrifugation, the obtained MagNP@PDA@AuNPs were stored in DMF.

### Synthesis of ZIF-8 Nanoparticles

Nanosized ZIF-8 particles were prepared by mixing 5 mL of MeOH solution of $Zn(NO_3)_2$ (12.5 mM) with 5 mL of MeOH solution of 2-methylimidazole (25 mM). The mixture was shaken for 10 s, and then allowed to react at room temperature for 12 h. The product was collected by centrifugation, washed several times with MeOH, and dried under a vacuum overnight.

### Synthesis of UiO-66 Nanoparticles

Nanosized UiO-66 particles were prepared by dissolving 4 mM $ZrCl_4$ and 4 mM $H_2BDC$ in a mixture of DMF and EtOH containing acetic acid. The reaction vial was capped and placed into an oven preheated at 100 °C for 12 h. The product was collected by centrifugation and then washed three times with DMF. The product was suspended in MeOH, and maintained at 60 °C for 3 days. MeOH was renewed every 24 h to remove DMF. Finally, the product was washed 3 times with MeOH.

### Synthesis of NP@PDA@ZIF-8 Nanoparticles

Typically, a predetermined amount of AuNP@PDA in MeOH was added into 3 mL of MeOH solution of $Zn(NO_3)_2$ (12.5 mM), followed by 3 mL of MeOH solution of 2-methylimidazole (25 mM). The mixture was shaken for 10 s, and then allowed to react at room temperature for 12 h. The pink product was collected by centrifugation and washed 3 times with MeOH before dried under a vacuum overnight. Similar procedure and conditions were used to coat ZIF-8 on other nanoparticles.

### Synthesis of NP@PDA@UiO-66 Nanoparticles

Typically, a predetermined amount of AuNP@PDA in DMF was added into a mixture of 4 mM $ZrCl_4$ and 4 mM $H_2BDC$ in a DMF–EtOH (v/v = 5:3) mixture. Afterward, the solution was treated by ultrasonication for 10 min. Subsequently, the vial was capped and placed into an oven preheated at 100 °C for 12 h. The pink product was collected by centrifugation and then washed three times with DMF. The product was soaked in MeOH at 60 °C for 3 days, and MeOH was renewed every 24 h to remove DMF. Finally, the product was washed 3 times with MeOH.

### Catalytic Study on 4-Nitrophenol

The rate of catalytic reaction was determined using UV–vis spectroscopy. For this purpose, 4-nitrophenol (1.5 mL, 0.2 mM) was mixed with fresh $NaBH_4$ solution (1.5 mL, 15 mM). 50 $\mu$L of different catalysts were added into the reaction mixture at room temperature. The absorbance spectra was recorded in the range of 350 to 800 nm.

### Catalytic Study on Methylene Blue

The rate of catalytic reaction was determined using UV–vis spectroscopy. For this purpose, methylene (1.5 mL, 8 mg/L) was mixed with fresh $NaBH_4$ solution (1.5 mL, 15 mM). 50 $\mu$L of different catalysts were added into the reaction mixture at room temperature. The absorbance spectra was recorded in the range of 400 to 750 nm.

## Supplementary Material

Refer to Web version on PubMed Central for supplementary material.

## Acknowledgments

## REFERENCES AND NOTES

1. Bigall NC, Parak WJ, Dorfs D. Fluorescent, Magnetic and Plasmonic—Hybrid Multifunctional Colloidal Nano Objects. Nano Today. 2012; 7:282–296.

2. Ghosh Chaudhuri R, Paria S. Core/Shell Nanoparticles: Classes, Properties, Synthesis Mechanisms, Characterization, and Applications. Chem Rev. 2012; 112:2373–2433. [PubMed: 22204603]

3. Liu Y, Tang Z. Multifunctional Nanoparticle@MOF Core–Shell Nanostructures. Adv Mater. 2013; 25:5819–5825. [PubMed: 24038572]

4. Jin Y, Jia C, Huang SW, O'Donnell M, Gao X. Multi-functional Nanoparticles as Coupled Contrast Agents. Nat Commun. 2010; 1:41. [PubMed: 20975706]

5. Huang X, Li Y, Chen Y, Zhou H, Duan X, Huang Y. Plasmonic and Catalytic AuPd Nanowheels for the Efficient Conversion of Light into Chemical Energy. Angew Chem, Int Ed. 2013; 52:6063–6067.

6. Liu N, Prall BS, Klimov VI. Hybrid Gold/Silica/Nanocrystal-Quantum-Dot Superstructures: Synthesis and Analysis of Semiconductor-Metal Interactions. J Am Chem Soc. 2006; 128:15362–15363. [PubMed: 17131988]

7. Jiang N, Shao L, Wang J. (Gold Nanorod Core)/(Polyaniline Shell) Plasmonic Switches with Large Plasmon Shifts and Modulation Depths. Adv Mater. 2014; 26:3282–3289. [PubMed: 24591117]

8. Deng Y, Cai Y, Sun Z, Liu J, Liu C, Wei J, Li W, Wang Y, Zhao D. Multifunctional Mesoporous Composite Micro-spheres with Well-Designed Nanostructure: A Highly Integrated Catalyst System. J Am Chem Soc. 2010; 132:8466–8473. [PubMed: 20507122]

9. Xing L, Cao YY, Che SA. Synthesis of Core–Shell Coordination Polymer Nanoparticles (CPNs) for pH-Responsive Controlled Drug Release. Chem Commun. 2012; 48:5995–5997.

10. Hao R, Xing R, Xu Z, Hou Y, Gao S, Sun S. Synthesis, Functionalization, and Biomedical Applications of Multi-functional Magnetic Nanoparticles. Adv Mater. 2010; 22:2729–2742. [PubMed: 20473985]

11. Zhou HC, Long JR, Yaghi OM. Introduction to Metal–Organic Frameworks. Chem Rev. 2012; 112:673–674. [PubMed: 22280456]

12. Couck S, Denayer JF, Baron GV, Remy T, Gascon J, Kapteijn F. An Amine-Functionalized MIL-53 Metal-Organic Framework with Large Separation Power for $CO_2$ and $CH_4$. J Am Chem Soc. 2009; 131:6326–6367. [PubMed: 19374416]

13. Kreno LE, Leong K, Farha OK, Allendorf M, Van Duyne RP, Hupp JT. Metal–Organic Framework Materials as Chemical Sensors. Chem Rev. 2012; 112:1105–1125. [PubMed: 22070233]

14. Lee J, Farha OK, Roberts J, Scheidt KA, Nguyen ST, Hupp JT. Metal–Organic Framework Materials as Catalysts. Chem Soc Rev. 2009; 38:1450–1459. [PubMed: 19384447]

15. DeCoste JB, Peterson GW. Metal–Organic Frameworks for Air Purification of Toxic Chemicals. Chem Rev. 2014; 114:5695–5727. [PubMed: 24750116]

16. Herm ZR, Swisher JA, Smit B, Krishna R, Long JR. Metal–Organic Frameworks as Adsorbents for Hydrogen Purification and Precombustion Carbon Dioxide Capture. J Am Chem Soc. 2011; 133:5664–5667. [PubMed: 21438585]

17. Farrusseng D, Aguado S, Pinel C. Metal–Organic Frameworks: Opportunities for Catalysis. Angew Chem, Int Ed. 2009; 48:7502–7513.

18. Li JR, Kuppler RJ, Zhou HC. Selective Gas Adsorption and Separation in Metal–Organic Frameworks. Chem Soc Rev. 2009; 38:1477–1504. [PubMed: 19384449]

19. Moon HR, Lim DW, Suh MP. Fabrication of Metal Nanoparticles in Metal–Organic Frameworks. Chem Soc Rev. 2013; 42:1807–1824. [PubMed: 23192676]

20. Zhu QL, Xu Q. Metal–Organic Framework Composites. Chem Soc Rev. 2014; 43:5468–5512. [PubMed: 24638055]

21. Houk RJ, Jacobs BW, El Gabaly F, Chang NN, Talin AA, Graham DD, House SD, Robertson IM, Allendorf MD. Silver Cluster Formation, Dynamics, and Chemistry in Metal–Organic Frameworks. Nano Lett. 2009; 9:3413–3418. [PubMed: 19757817]

22. Hermes S, Schroter MK, Schmid R, Khodeir L, Muhler M, Tissler A, Fischer RW, Fischer RA. Metal@MOF: Loading of Highly Porous Coordination Polymers Host Lattices by Metal Organic Chemical Vapor Deposition. Angew Chem, Int Ed. 2005; 44:6237–6241.

23. Wang C, deKrafit KE, Lin W. Pt Nanoparticles@ Photoactive Metal–Organic Frameworks: Efficient Hydrogen Evolution *via* Synergistic Photoexcitation and Electron Injection. J Am Chem Soc. 2012; 134:7211–7214. [PubMed: 22486151]

24. Aijaz A, Karkamkar A, Choi YJ, Tsumori N, Ronnebro E, Autrey T, Shioyama H, Xu Q. Immobilizing Highly Catalytically Active Pt Nanoparticles inside the Pores of Metal–Organic Framework: A Double Solvents Approach. J Am Chem Soc. 2012; 134:13926–13929. [PubMed: 22888976]

25. Buso D, Jasieniak J, Lay MD, Schiavuta P, Scopece P, Laird J, Amenitsch H, Hill AJ, Falcaro P. Highly Luminescent Metal–Organic Frameworks through Quantum Dot Doping. Small. 2012; 8:80–88. [PubMed: 22009888]

26. Doherty CM, Buso D, Hill AJ, Furukawa S, Kitagawa S, Falcaro P. Using Functional Nano- and Microparticles for the Preparation of Metal–Organic Framework Composites with Novel Properties. Acc Chem Res. 2014; 47:396–405. [PubMed: 24205847]

27. Lu G, Li S, Guo Z, Farha OK, Hauser BG, Qi X, Wang Y, Wang X, Han S, Liu X, et al. Imparting Functionality to a Metal–Organic Framework Material by Controlled Nanoparticle Encapsulation. Nat Chem. 2012; 4:310–316. [PubMed: 22437717]

28. Zhang W, Lu G, Cui C, Liu Y, Li S, Yan W, Xing C, Chi YR, Yang Y, Huo F. A Family of Metal–Organic Frameworks Exhibiting Size-Selective Catalysis with Encapsulated Noble-Metal Nanoparticles. Adv Mater. 2014; 26:4056–4060. [PubMed: 24710716]

29. Sugikawa K, Nagata S, Furukawa Y, Kokado K, Sada K. Stable and Functional Gold Nanorod Composites with a Metal–Organic Framework Crystalline Shell. Chem Mater. 2013; 25:2565–2570.

30. He L, Liu Y, Liu J, Xiong Y, Zheng J, Tang Z. Core–Shell Noble-Metal@Metal–Organic Framework Nanoparticles with Highly Selective Sensing Property. Angew Chem, Int Ed. 2013; 52:3741–3745.

31. Zhao M, Deng K, He L, Liu Y, Li G, Zhao H, Tang Z. Core–Shell Palladium Nanoparticle@Metal–Organic Frameworks as Multifunctional Catalysts for Cascade Reactions. J Am Chem Soc. 2014; 136:1738–1741. [PubMed: 24437922]

32. Zhang Z, Chen Y, Xu X, Zhang J, Xiang G, He W, Wang X. Well-Defined Metal–Organic Framework Hollow Nanocages. Angew Chem, Int Ed. 2014; 53:429–433.

33. Sindoro M, Granick S. Voids and Yolk–Shells from Crystals that Coat Particles. J Am Chem Soc. 2014; 136:13471–13473. [PubMed: 25243973]

34. Zhang W, Wu ZY, Jiang HL, Yu SH. Nanowire-Directed Templating Synthesis of Metal–Organic Framework Nanofibers and Their Derived Porous Doped Carbon Nanofibers for Enhanced Electrocatalysis. J Am Chem Soc. 2014; 136:14385–14388. [PubMed: 25244060]

35. Hu P, Zhuang J, Chou LY, Lee HK, Ling XY, Chuang YC, Tsung CK. Surfactant-Directed Atomic to Mesoscale Alignment: Metal Nanocrystals Encased Individually in Single-Crystalline Porous Nanostructures. J Am Chem Soc. 2014; 136:10561–10564. [PubMed: 25007206]

36. Zhou J, Duan B, Fang Z, Song J, Wang C, Messersmith PB, Duan H. Interfacial Assembly of Mussel-Inspired Au@Ag@Polydopamine Core–Shell Nanoparticles for Recyclable Nanocatalysts. Adv Mater. 2014; 26:701–705. [PubMed: 24493052]

37. Lee H, Dellatore SM, Miller WM, Messersmith PB. Mussel-Inspired Surface Chemistry for Multifunctional Coatings. Science. 2007; 318:426–430. [PubMed: 17947576]

38. Kim BH, Lee DH, Kim JY, Shin DO, Jeong HY, Hong S, Yun JM, Koo CM, Lee H, Kim SO. Mussel-Inspired Block Copolymer Lithography for Low Surface Energy Materials of Teflon, Graphene, and Gold. Adv Mater. 2011; 23:5618–5622. [PubMed: 22021119]

39. Sedo J, Saiz-Poseu J, Busque F, Ruiz-Molina D. Catechol-Based Biomimetic Functional Materials. Adv Mater. 2013; 25:653–701. [PubMed: 23180685]

40. Saiz-Poseu J, Sedo J, Garcia B, Benaiges C, Parella T, Alibes R, Hernando J, Busque F, Ruiz-Molina D. Versatile Nanostructured Materials *via* Direct Reaction of Functionalized Catechols. Adv Mater. 2013; 25:2066–2070. [PubMed: 23418006]

41. Lee YH, Lee H, Kim YB, Kim JY, Hyeon T, Park H, Messersmith PB, Park TG. Bioinspired Surface Immobilization of Hyaluronic Acid on Monodisperse Magnetite Nanocrystals for Targeted Cancer Imaging. Adv Mater. 2008; 20:4154–4157. [PubMed: 19606262]

42. Lee Y, Lee H, Messersmith PB, Park TG. A Bioinspired Polymeric Template for 1D Assembly of Metallic Nanoparticles, Semiconductor Quantum Dots, and Magnetic Nanoparticles. Macromol Rapid Commun. 2010; 31:2109–2114. [PubMed: 21567637]

43. Guo J, Ping Y, Ejima H, Alt K, Meissner M, Richardson JJ, Yan Y, Peter K, von Elverfeldt D, Hagemeyer CE, et al. Engineering Multifunctional Capsules through the Assembly of Metal-Phenolic Networks. Angew Chem, Int Ed. 2014; 53:5546–5551.

44. Liu Q, Wang N, Caro J, Huang A. Bio-Inspired Polydopamine: A Versatile and Powerful Platform for Covalent Synthesis of Molecular Sieve Membranes. J Am Chem Soc. 2013; 135:17679–17682. [PubMed: 24224527]

45. Ye Q, Zhou F, Liu W. Bioinspired Catecholic Chemistry for Surface Modification. Chem Soc Rev. 2011; 40:4244–4258. [PubMed: 21603689]

46. Black KC, Liu Z, Messersmith PB. Catechol Redox Induced Formation of Metal Core-Polymer Shell Nanoparticles. Chem Mater. 2011; 23:1130–1135. [PubMed: 21666825]

47. Lee M, Kim JU, Lee JS, Lee BI, Shin J, Park CB. Mussel-Inspired Plasmonic Nanohybrids for Light Harvesting. Adv Mater. 2014; 26:4463–4468. [PubMed: 24623446]

48. Zhang L, Wu J, Wang Y, Long Y, Zhao N, Xu J. Combination of Bioinspiration: A General Route to Super-hydrophobic Particles. J Am Chem Soc. 2012; 134:9879–9881. [PubMed: 22656181]

49. Anker JN, Hall WP, Lyandres O, Shah NC, Zhao J, Van Duyne RP. Biosensing with Plasmonic Nanosensors. Nat Mater. 2008; 7:442–453. [PubMed: 18497851]

50. Song J, Zhou J, Duan H. Self-Assembled Plasmonic Vesicles of SERS-Encoded Amphiphilic Gold Nanoparticles for Cancer Cell Targeting and Traceable Intracellular Drug Delivery. J Am Chem Soc. 2012; 134:13458–13469. [PubMed: 22831389]

51. Barbosa S, Agrawal A, Rodriguez-Lorenzo L, Pastoriza-Santos I, Alvarez-Puebla RA, Kornowski A, Weller H, Liz-Marzan LM. Tuning Size and Sensing Properties in Colloidal Gold Nanostars. Langmuir. 2010; 26:14943–14650. [PubMed: 20804155]

52. Sreejith S, Ma X, Zhao Y. Graphene Oxide Wrapping on Squaraine-Loaded Mesoporous Silica Nanoparticles for Bioimaging. J Am Chem Soc. 2012; 134:17346–17349. [PubMed: 22799451]

53. Deng Z, Chen M, Gu G, Wu L. A Facile Method to Fabricate ZnO Hollow Spheres and Their Photocatalytic Property. J Phys Chem B. 2008; 112:16–22. [PubMed: 18067281]

54. Xu H, Cui L, Tong N, Gu H. Development of High Magnetization $Fe_3O_4$/Polystyrene/Silica Nanospheres *via* Combined Miniemulsion/Emulsion Polymerization. J Am Chem Soc. 2006; 128:15582–15583. [PubMed: 17147355]

55. Probst CE, Zrazhevskiy P, Gao X. Rapid Multitarget Immunomagnetic Separation through Programmable DNA Linker Displacement. J Am Chem Soc. 2011; 133:17126–17129. [PubMed: 21988124]

56. Wu W, Kirillov AM, Yan X, Zhou P, Liu W, Tang Y. Enhanced Separation of Potassium Ions by Spontaneous K+-Induced Self-Assembly of a Novel Metal–Organic Framework and Excess Specific Cation-pi Interactions. Angew Chem, Int Ed. 2014; 53:10649–10653.
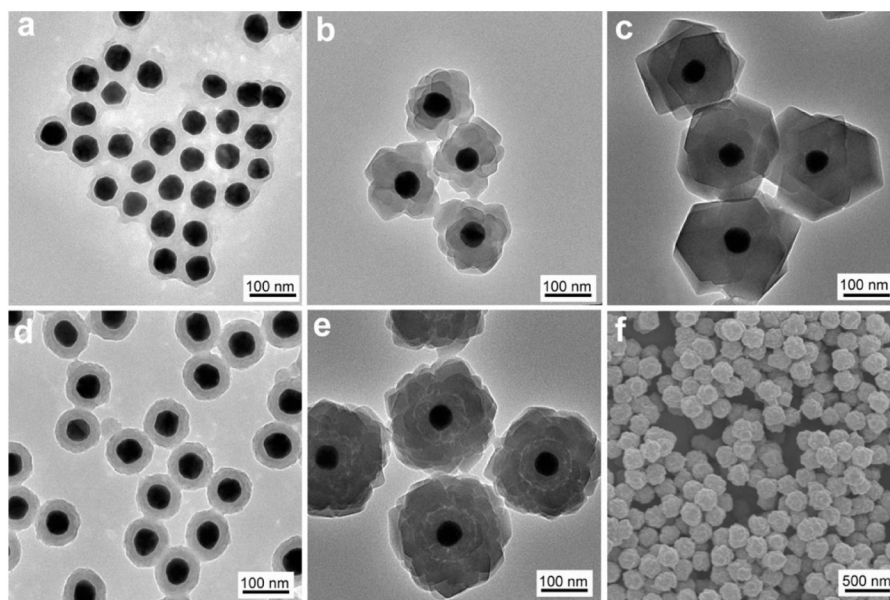
**Figure 1.**
(a–c) TEM images of AuNP@PDA with a 6 nm PDA layer, and corresponding AuNP@PDA@ZIF-8 with 40 and 90 nm ZIF-8 shell. (d,e) TEM images of AuNP@PDA with a 25 nm PDA layer and corresponding AuNP@PDA@ZIF-8. (f) SEM image of AuNP@PDA@ZIF-8.
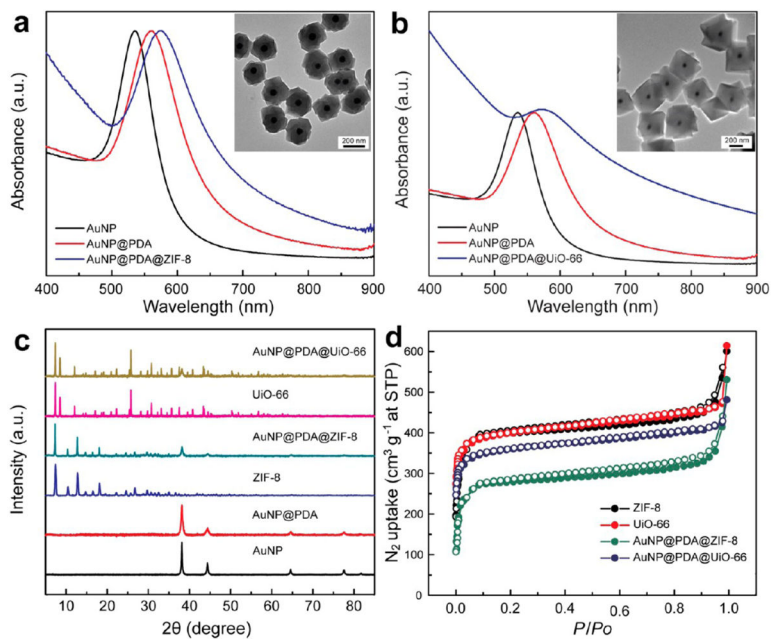
**Figure 2.**
(a) UV–vis spectra of Au nanoparticle, AuNP@PDA, and AuNP@PDA@ZIF-8. Inset: TEM image of AuNP@PDA@ZIF-8. (b) UV–vis spectra of Au nanoparticle, AuNP@PDA, and AuNP@PDA@UiO-66. Inset: TEM image of AuNP@PDA@UiO-66. (c) XRD patterns of different samples. (d) Nitrogen-sorption isotherms for different samples at 77 K up to 1 bar. The solid and open symbols represent adsorption and desorption, respectively.
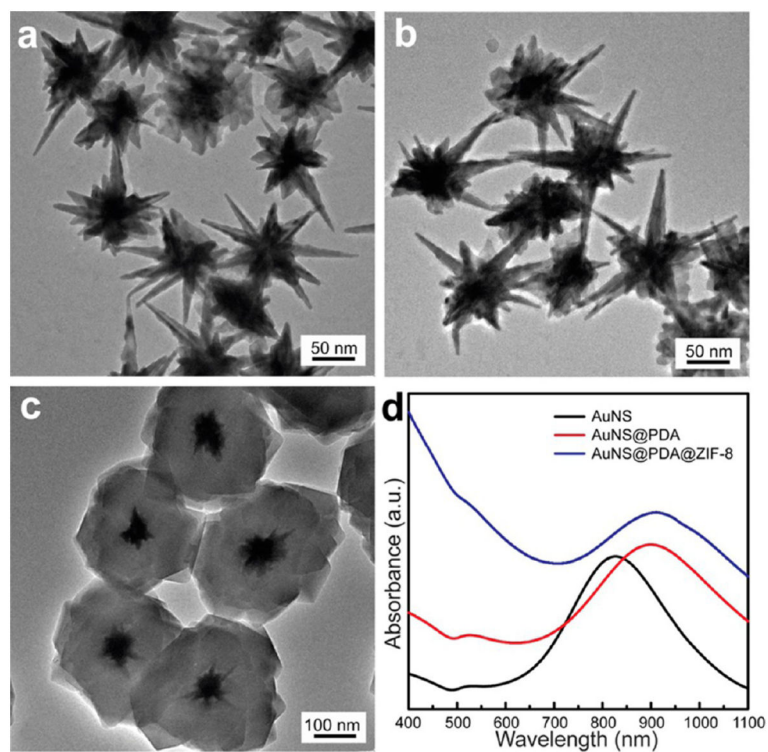
**Figure 3.**
TEM images of (a) Au nanostars (AuNSs), (b) AuNS@PDA, (c) AuNS@PDA@ZIF-8. (d) UV–vis spectra of different materials.
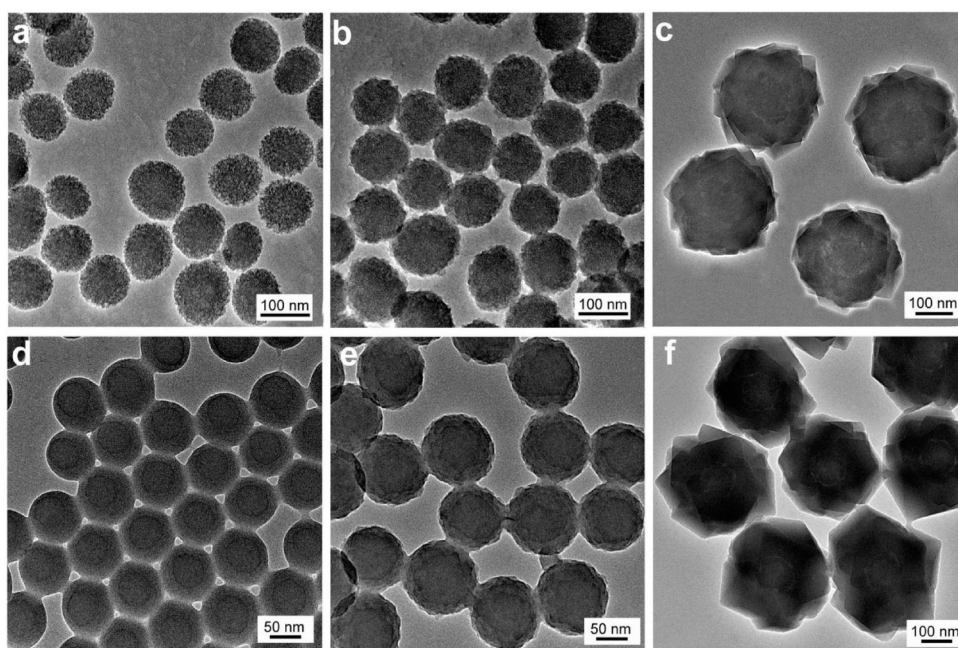
**Figure 4.**
TEM images of (a) MSN, (b) MSN@PDA, (c) MSN@PDA@ZIF-8, (d) PSN, (e) PSN@PDA, (f) PSN@PDA@ZIF-8.
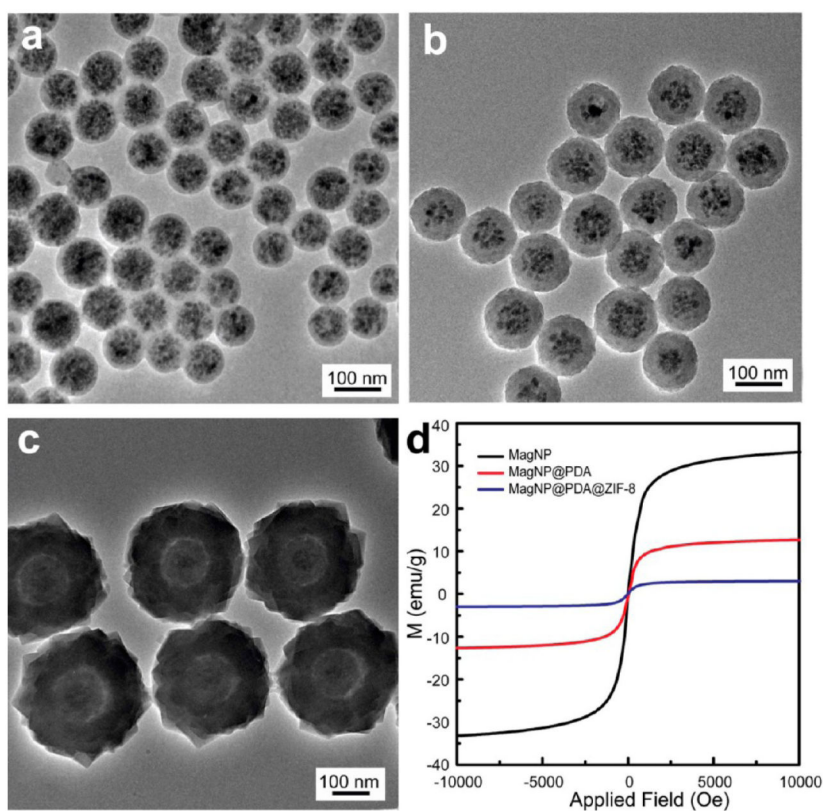
**Figure 5.**
TEM images of (a) MagNP, (b) MagNP@PDA, (c) MagNP@PDA@ZIF-8. (d)
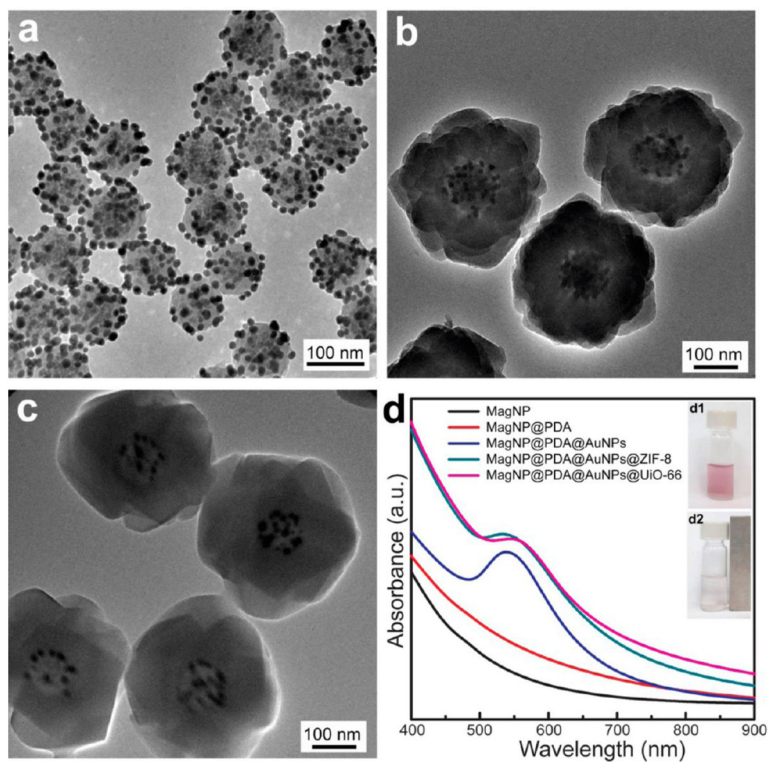Magnetization curves at 300 K of different materials.

**Figure 6.**
TEM images of (a) MagNP@PDA@AuNPs, and MagNP@PDA@AuNPs coated with (b) ZIF-8 and (c) UiO-66. (d) UV–vis spectra of different materials. Inset: photographs of MagNP@PDA@AuNPs@MOF before (d1) and after (d2) magnetic separation.
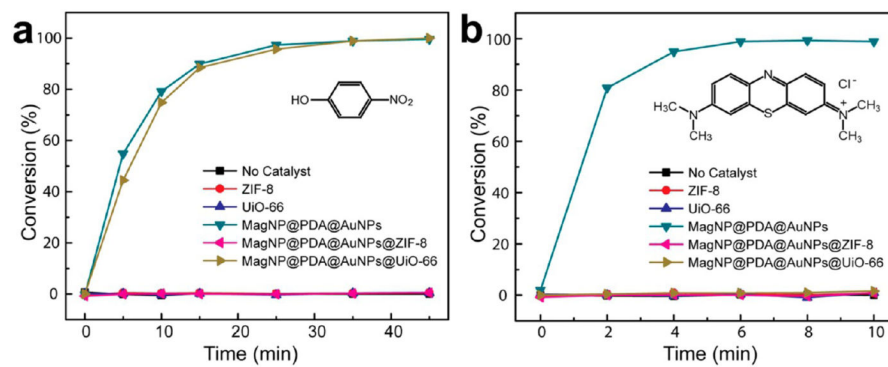
**Figure 7.**
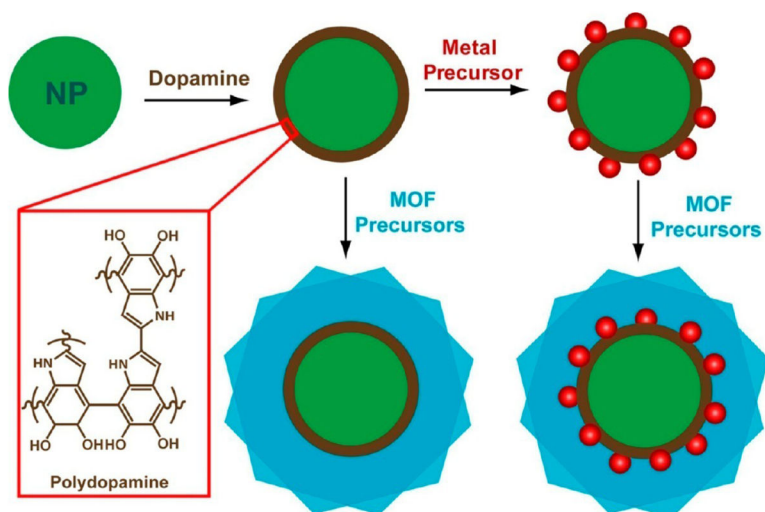Reaction kinetics of the conversion of (a) 4-NPh and (b) MB catalyzed by various materials.

**Scheme 1.**
Illustration of the stepwise synthesis of nanoparticle@PDA, nanoparticle@PDA@MOF, and metal nanocatalyst-loaded nanoparticle@PDA@MOF core–shell hybrid nanostructures.